Supporting Information

Core-Linked Dimer Acceptors with Flexible Linker for High-efficiency and Robust Organic Solar Cells

Pengchao Zhang,† Hongna Zhang,† Shuzhe Liu, Feng Qi, Yetai Cheng, Guangliu Ran, Jianqi Zhang, Hao Lu*, Wenkai Zhang, Zhishan Bo* and Yahui Liu**

P. Zhang, S. Liu, F. Qi, Y. Cheng, H. Lu, Y. Liu,
College of Textiles & Clothing, State Key Laboratory of Bio-fibers and Eco-textiles, Qingdao University, Qingdao 266071, China
E-mail: qifeng@qdu.edu.cn; luhao@qdu.edu.cn; liuyh@qdu.edu.cn

H. Zhang
School of Public Health, Qingdao University, Qingdao 266071, China

F. Qi, H. Lu
College of Materials Science and Engineering, Qingdao University, Qingdao 266071, China

G. Ran, W. Zhang
Department of Physics and Applied Optics Beijing Area Major Laboratory, Beijing Normal University, Beijing 100875, China

J. Zhang
CAS Key Laboratory of Nanosystem and Hierarchical Fabrication, National Center for Nanoscience and Technology, Beijing 100190, China

Z. Bo
Beijing Key Laboratory of Energy Conversion and Storage Materials, College of Chemistry, Beijing Normal University, Beijing 100875, China
E-mail: zsbo@bnu.edu.cn

† P. Zhang and H. Zhang contributed equally to the work.

Materials: All chemicals and reagents were purchased from commercial companies and were used without further purification.

Measurements: The ^{1}H NMR spectra were obtained using a Bruker 600 MHz AVANCE III spectrometer with $CDCl_3$ as the solvent. UV-Vis absorption spectra were recorded using a HITACHI UH5700 Ultra-Violet Visible Scanning Spectrophotometer. In-situ UV-vis absorption measurements were carried out with a Filmetrics F20-EXR spectrometer in transmission mode, with a time resolution of 0.05 seconds. The setup includes a light source positioned above the substrate and a detector positioned below it, aligned vertically. The solution was spin-coated onto the substrate, creating a film on the glass surface, and during the coating process, the detector captured transmission spectra ranging from 300 to 1000 nm. Cyclic voltammetry (CV) was performed using a CHI660E electrochemical analyzer system with an anhydrous acetonitrile solution of tetra-*n*-butylammonium hexafluorophosphate (Bu_4NPF_6) (0.1 M), at a scan rate of 50 mV s^{-1}. A conventional three-electrode system was used, with a glassy carbon electrode as the working electrode, a platinum wire as the counter electrode, and an Ag/AgCl electrode as the reference electrode. Additionally, $FeCp_2/FeCp_2^+$ was used as an internal reference. The contact angle was measured using a Biolin Theta instrument. Atomic force microscopy (AFM) images were captured with a Bruker Multimode 8 microscope. Grazing incidence wide-angle X-ray scattering (GIWAXS) measurements were conducted at beamline 7.3.3 at the Advanced Light Source. Differential scanning calorimetry (DSC) was conducted on a Mettler-Toledo-DSC3 analyzer at a heating and cooling rate of 5 and 10 K min^{-1}. Glass transition temperature (T_g) of film samples was obtained by extracting the deviation metric (DM) from the temperature-dependent absorption spectra. Here, DM can be calculated based on the equation described as：

$$DM_T = \sum_{\lambda_{min}}^{\lambda_{max}} (I_{RT}(\lambda) - I_T(\lambda))^2$$

where $I_{RT}(\lambda)$ and $I_T(\lambda)$ represent the absorption intensity of as-cast and annealed acceptor films, respectively.

Materials Synthesis

Synthesis of Compound 3

Under a nitrogen atmosphere, lithium aluminum hydride ($LiAlH_4$; 534 mg, 10.4 mmol) was added to a solution of compound 1 (968 mg, 0.7 mmol) in tetrahydrofuran (THF; 30 mL). The mixture was stirred and refluxed overnight. After cooling to room temperature, the solution was slowly quenched with water and extracted with chloroform. The organic phase was dried over anhydrous magnesium sulfate ($MgSO_4$), filtered, and concentrated by rotary evaporation. The crude product was dissolved in acetic acid (15 mL) and ethanol (15 mL), then 3-bromo-9,10-anthraquinone (1004 mg, 3.5 mmol) was added. The reaction mixture was stirred at room temperature overnight. The organic phase was washed with deionized water, extracted with chloroform, dried over anhydrous $MgSO_4$, and filtered. The solvent was removed by rotary evaporation. The concentrated crude product was purified by silica gel column chromatography using hexane/chloroform (9:1, v/v) as the eluent, yielding a purplish-red solid (666 mg, 60%).^{1}H NMR (600 MHz, Chloroform-d) δ = 9.78 (d, 1H), 9.58 (d, 1H), 8.80 (s, 1H), 8.60 (d, 1H), 8.01 (d, 1H), 7.93 (t, 1H), 7.83 (t, 1H), 7.03 (s, 2H), 4.68 (d, 4H), 2.93 (t, 4H), 2.17 (m,2 H), 1.94 (m, 4H), 1.55-1.50 (m, 10H), 1.45-1.41 (m, 4H), 1.36-1.32 (m, 6H), 1.31-1.28 (m, 10H), 1.24-1.20 (m, 12H), 1.18-1.14 (m, 12H), 1.08-1.03 (m, 16H), 0.97-0.94 (m, 14H), 0.89-0.84 (m, 32H), 0.81-0.79 (m, 6H).

Synthesis of Compound 4

Under a nitrogen atmosphere, compound 3 (634 mg, 0.4 mmol), anhydrous chloroform (30 mL), and anhydrous N,N-dimethylformamide (DMF; 7.5 mL) were prepared and stirred at room temperature for 1 hour. Phosphorus oxychloride ($POCl_3$; 0.75 mL) was then added dropwise to the mixture and refluxed overnight. The mixture was quenched with water for 2 hours, then extracted with chloroform. The organic phase was dried over anhydrous magnesium sulfate ($MgSO_4$), filtered, and concentrated by rotary evaporation. The concentrated crude product was purified by column chromatography using hexane/chloroform (2:8, v/v) as the eluent, yielding a red solid (591 mg, 90%). ^{1}H NMR (600 MHz, Chloroform-*d*) δ = 10.18 (d, 2H), 9.68 (d, 1H),

9.54 (d, 1H),, 8.82 (s, 1H), 8.62 (d, 1H), 8.03 (d, 1H), 7.96 (s, 1H), 7.88 (s, 1H), 4.72 (s, 4H), 2.93 (t, 4H), 3.31 (s,2 H), 2.18 (s, 2H), 2.01 (s, 4H),1.55 (s, 14H), 1.44 (m, 6H), 1.33-1.28 (m, 10H), 1.22-1.12 (m, 30H), 0.97-0.82 (m, 30H), 0.81-0.78 (m, 6H).

Synthesis of PQx-F

Under nitrogen conditions, compound 6 (150 mg, 0.091 mmol) and IC-2F (46.0 mg, 0.2 mmol) were added to a round-bottom flask and dissolved in anhydrous toluene (15 mL). Acetic anhydride (Ac_2O; 0.07 mL) and boron trifluoride etherate ($BF_3 \cdot OEt_2$; 0.13 mL, 1 mmol) were then added sequentially, and the mixture was stirred at room temperature for 30 minutes. The organic phase was washed with deionized water, extracted with chloroform, and dried over anhydrous magnesium sulfate ($MgSO_4$) before being filtered. The residual solvent was removed by rotary evaporation. The crude product was purified by silica gel column chromatography using hexane/chloroform (1:9, v/v) as the eluent, yielding a black solid, PQx-F (160 mg, 85%). ^{1}H NMR (600 MHz, Chloroform-*d*) δ = 9.50 (d, 1H), 9.30 (d, 1H), 9.14 (d, 2H), 8.70 (s, 1H), 8.50 (m, 3H), 7.93 (d, 1H), 7.85 (t, 2H), 7.68 (s, 2H), 4.89 (d, 4H), 3.30 (t, 4H), 2.27 (s,2 H), 1.95 (m, 4H), 1.58 (m, 4H), 1.48 (m, 10H), 1.43 (m, 4H), 1.37-1.31 (m, 6H), 1.30-1.23 (m, 16H), 1.20-1.17 (m, 8H), 1.14-1.10 (m, 16H), 1.05-1.04 (m, 14H), 1.01-0.92 (m, 24H), 0.87-0.84 (m, 8H), 0.82-0.80 (m, 8H), 0.77-0.74 (m, 6H).

Synthesis of *d*PQx-F

Compound PQx-F (100 mg, 0.048 mmol), 1,8-bis(5-(trimethylstannyl)thiophen-2-yl)octane (11.7 mg, 0.019 mmol), and tetrakis(triphenylphosphine)palladium ($Pd(PPh_3)_4$; 1 mg, 4 μmol) were dissolved in anhydrous toluene (20 mL) and placed in a nitrogen-filled double-neck round-bottom flask. The mixture was stirred and refluxed overnight. After cooling to room temperature, the organic phase was washed with deionized water, extracted with chloroform, dried over anhydrous magnesium sulfate ($MgSO_4$), and filtered. The residual solvent was removed by rotary evaporation. The crude product was purified by silica gel column chromatography using

hexane/chloroform (3:1, v/v) as the eluent, yielding a black solid, *d*PQx-F (61 mg, 60%). ^{1}H NMR (600 MHz, Chloroform-*d*) δ = 9.23 (=s, 2H), 9.09 (s, 2H), 9.01 (s, 4H), 8.46 (s, 4H), 8.42 (s, 2H), 8.37 (s, 2H), 7.91 (s, 2H), 7.71 (s, 2H), 7.65 (s, 2H), 7.58 (s, 2H), 7.39 (s,2 H), 7.33 (s, 2H), 6.85 (s, 2H), 4.92 (s, 8H), 3.26 (s, 4H), 3.16 (s, 4H), 2.95 (s, 4H), 2.36 (s, 4H), 1.94 (s, 4H), 1.83 (s, 8H), 1.52-1.41 (m, 36H), 1.34 (m, 24H), 1.26 (m, 18H), 1.23 (m, 24H), 1.16-0.99 (m,108 H), 0.83 (m, 6H), 0.79 (m, 24H), 0.74 (m, 16H).

Device fabrication and measurements

The device structure of ITO/2PACz/D18: acceptors /PDINN/Ag was fabri cated using a conventional device structure. The ITO/glass substrates were first cleaned with detergent, deionized water, acetone, and isopropyl alcohol, then dried in an oven at 110°C for 24 hours, followed by plasma treatment for 25 minutes. The ITO glass substrates were treated in plasma for 25 minutes. Then, a 2PACz layer was spin-coated onto the ITO substrates at 5000 rpm for 25 s and annealed in air at 70°C for 5 minutes. Next, a mixture of D18 and *d*PQx-F/L8-BO/PQx-F (weight ratio 1:1.2) was dissolved in chloroform, with a total concentration of 7 mg/mL for all blend solutions. 0.5% CN was added as an additive, and the mixture was stirred at 55°C on a hot plate for 2 hours in a nitrogen-filled glovebox. The solution was then spin-coated onto the 2PACz layer at 2000 rpm for 20 seconds, followed by annealing at 90°C for 5 minutes. After spin-coating the PDINN layer, a 90 nm thick Ag layer was sequentially deposited under high vacuum conditions. The current density-voltage (*J-V*) characteristics of the devices were measured using a Keithley 2400 source meter. Simulated sunlight was provided by an AM 1.5G solar simulator (Enlitech, Taiwan, model SS-F5), calibrated using a silicon diode calibrated by the National Renewable Energy Laboratory (NREL). Quantum efficiency curves were measured using a QE measurement system from Enlitech. The electroluminescence external quantum efficiency (EQE) spectra were obtained using a custom-built system that included a Hamamatsu silicon photodiode 1010B, a Keithley 2400 Source meter (for applying voltage and recording the injected current), and a Keithley 485 picoammeter (for measuring the emitted light intensity).

Femtosecond transient absorption experiments were conducted using a KGW laser (provided by Light Conversion, working wavelength 1030 nm, repetition frequency 54 kHz), which outputs two beams of light. One beam passed through an optical parametric amplifier (Orpheus, provided by Light Conversion) to generate high-intensity pulses of specific wavelengths as the pump light, while the other beam was focused on a 5 mm sapphire crystal to produce low-intensity continuous light as the probe light. The pump and probe beams overlapped spatially at a magic angle of 54.7°, and the time delay between the pump and probe beams was controlled using a delay stage, while the transmitted probe light was captured by a charge-coupled device (CCD). The pump light flux was maintained at ~2 μJ/cm². For thin film samples, six transient absorption experiments were conducted at different positions on each sample.

SCLC device fabrication and characterization

The electron-only devices were fabricated by the structure: ITO/ZnO/blend film/PNDNN/Al. The mobilities were calculated according to the equation listed below:

$$J = \frac{9\varepsilon_0\varepsilon_r\mu V^2}{8L^3}$$

where J is the current density, $\varepsilon 0$ is the vacuum permittivity, εr is the relative dielectric constant, μ is the mobility, V is the voltage, and L is the film thickness.

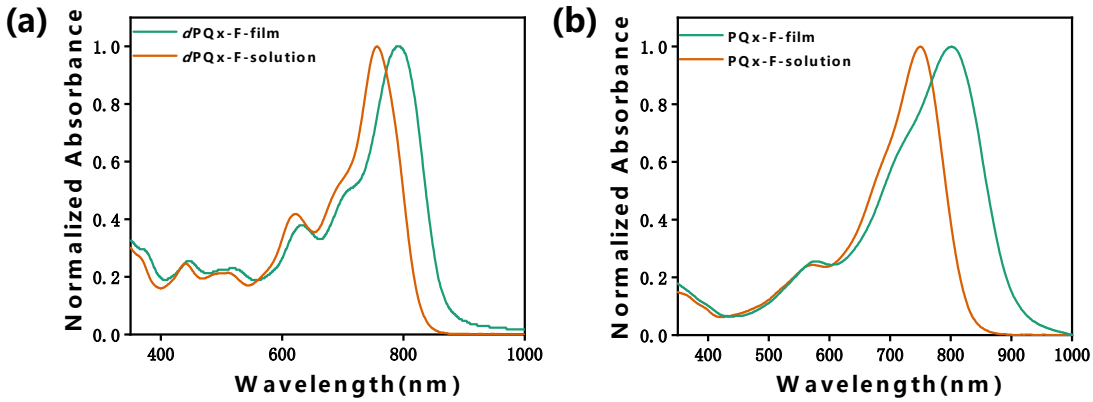

Figure S1. a) UV absorption spectrum of *d*PQx-F, b) UV absorption spectrum of

PQx-F.

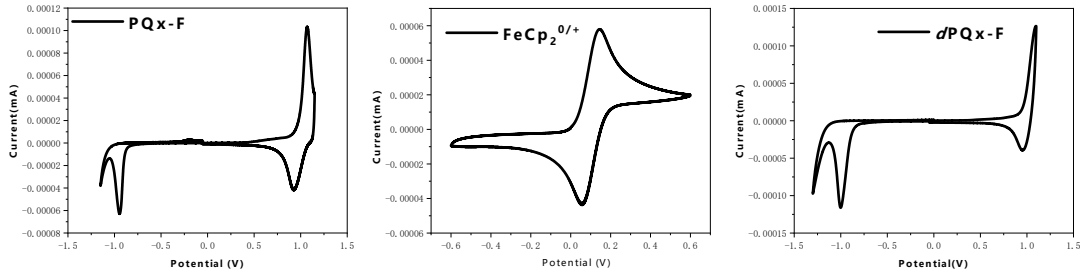

Figure S2. Electrochemical cyclic voltammogram curves of *d*PQx-F, PQx-F, and $FeCp_2^{0/+}$.

Table S1. Summary of Optical and Electrochemical Parameters of *d*PQx-F and PQx-F.

NFA	$\lambda_{f,max}$ a) [nm]	$\lambda_{s,max}$ b) [nm]	λ_{onset} c) [nm]	E_g^{opt} d) [eV]	HOMO e) [eV]	LUMO f) [eV]
*d*PQx-F	791	757	870	1.43	-5.64	-3.73
PQx-F	801	749	881	1.41	-5.69	-3.79

a) Absorption maximum in film, b)Absorption maximum in solution c) absorption edge in film, d) optical bandgap estimated from thin-film absorption e) HOMO energy level estimated from the onset oxidation potential, f) LUMO energy level estimated from the onset reduction potential.

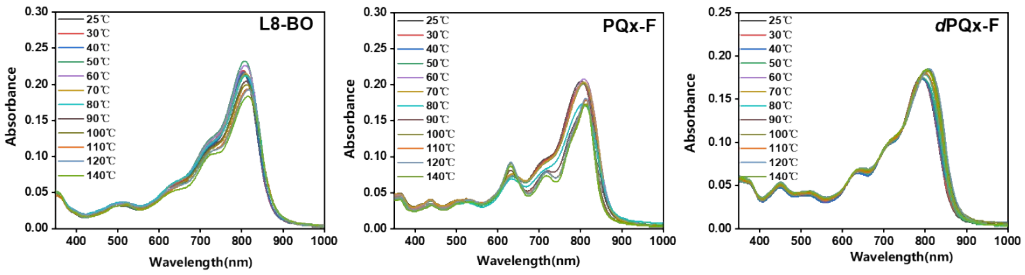

Figure S3. Film absorption measured under different temperatures for L8-BO, PQx-F and *d*PQx-F.

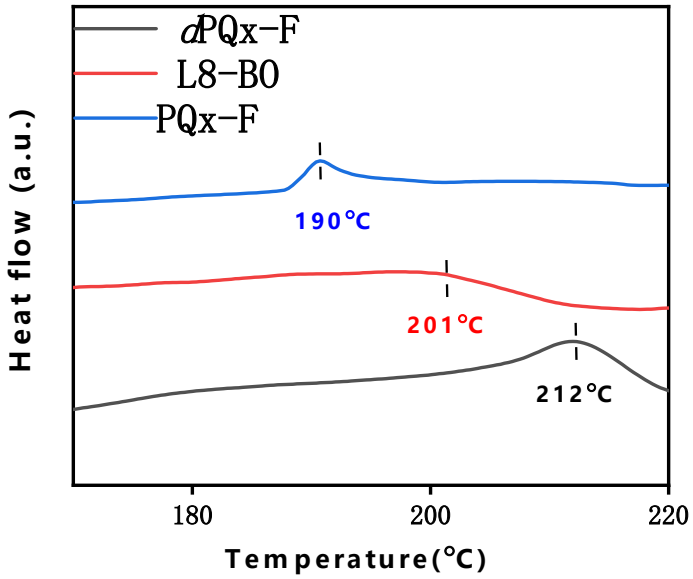

Figure S4. The DSC thermograms for L8-BO, PQx-F and *d*PQx-F.

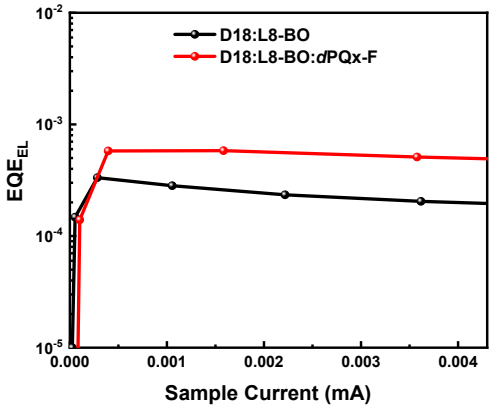

Figure S5. EQE_{EL} curves for the devices based on D18:L8-BO and D18:L8-BO:*d*PQx-F.

Table S2. The detailed parameters derived from the J_{ph}-V_{eff} curves.

	J_{sat}(mA/cm^2)	J_{ph}(mA/cm^2)	J_{max}(mA/cm^2)	P_{diss}(%)	P_{coll}(%)
D18:L8-BO	24.72	25.06	21.66	98.64	86.43
D18:PQx-F	18.91	19.25	15.36	98.23	79.79
D18:*d*PQx-F	14.32	14.94	9.86	95.85	66.00
D18:L8-BO:*d*PQx-F	25.24	25.34	23.01	99.60	90.80

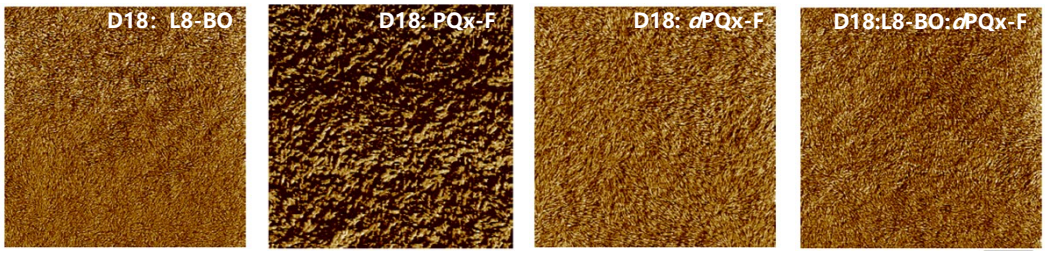

Figure S6. Phase diagram of D18:L8-BO, D18: PQx-F, D18: *d*PQx-F and D18:L8-BO: *d*PQx-F.

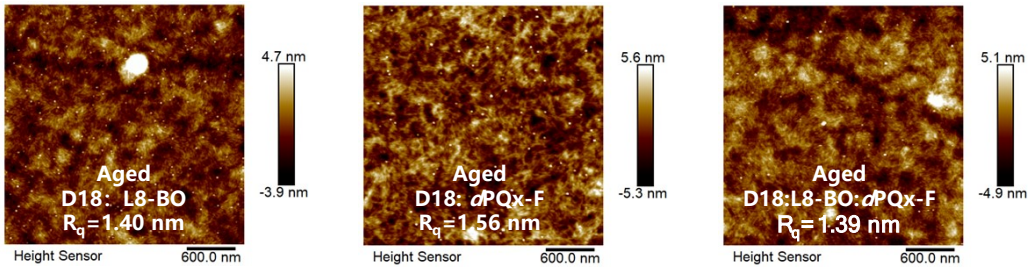

Figure S7. AFM height images of aged D18:L8-BO, D18: *d*PQx-F, and D18:L8-BO:*d*PQx-F films.

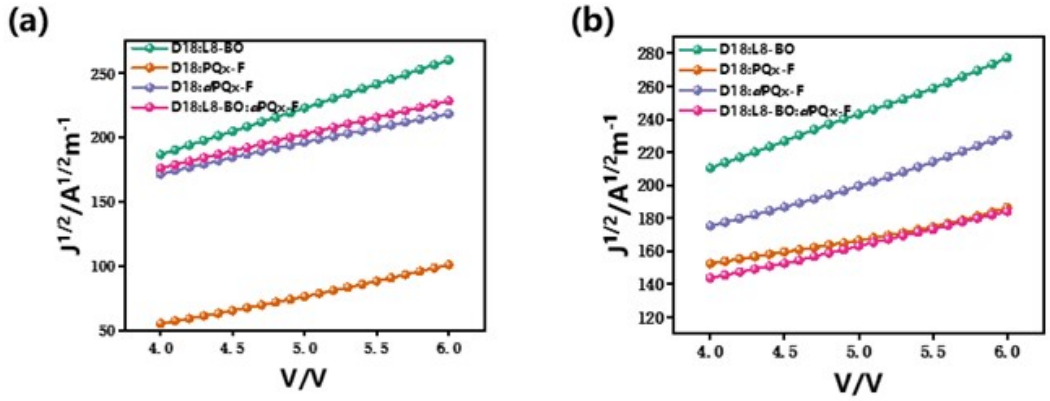

Figure S8. (a) Hole- and (b) elecreon-only devices of binary and ternary devices.

Table S3. Summary of SCLC characteristics of devices based on D18:L8-BO,D18: PQx-F,D18: *d*PQx-F and D18:L8-BO: *d*PQx-F.

	μ_e (cm^2 V^{-1} S^{-1})	μ_h (cm^2 V^{-1} S^{-1})	μ_e/μ_h
D18:L8-BO	4.82×10^{-4}	4.43×10^{-4}	1.08
D18:PQx-F	1.94×10^{-4}	3.88×10^{-4}	0.50
D18:*d*PQx-F	4.04×10^{-4}	4.38×10^{-4}	0.92
D18:L8-BO:*d*PQx-F	5.03×10^{-4}	4.79×10^{-4}	1.05

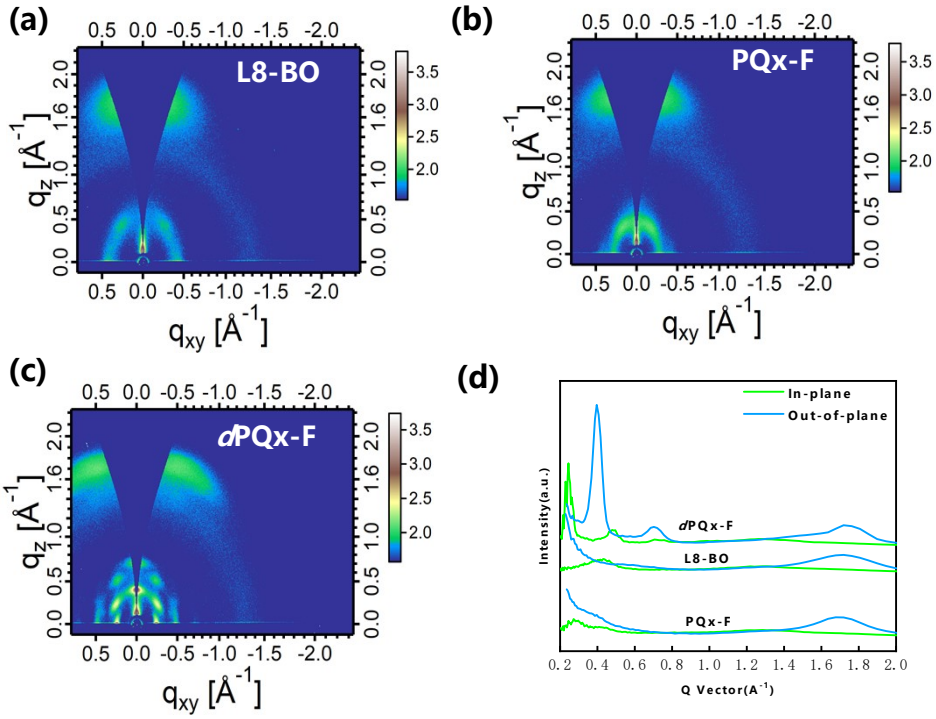

Figure S9. 2D GIWAXS of the L8-BO (a), PQx-F (b) and *d*PQx-F (c) blend films. (d) 1D GIWAXS patterns of the L8-BO, PQx-F and *d*PQx-F films.

Table S4. Summary of specific GIWAXS data for L8-BO, PQx-F and *d*PQx-F**.**

	L8BO	PQx-F	*d*PQx-F
CCL (Å)	14.30	19.80	19.72

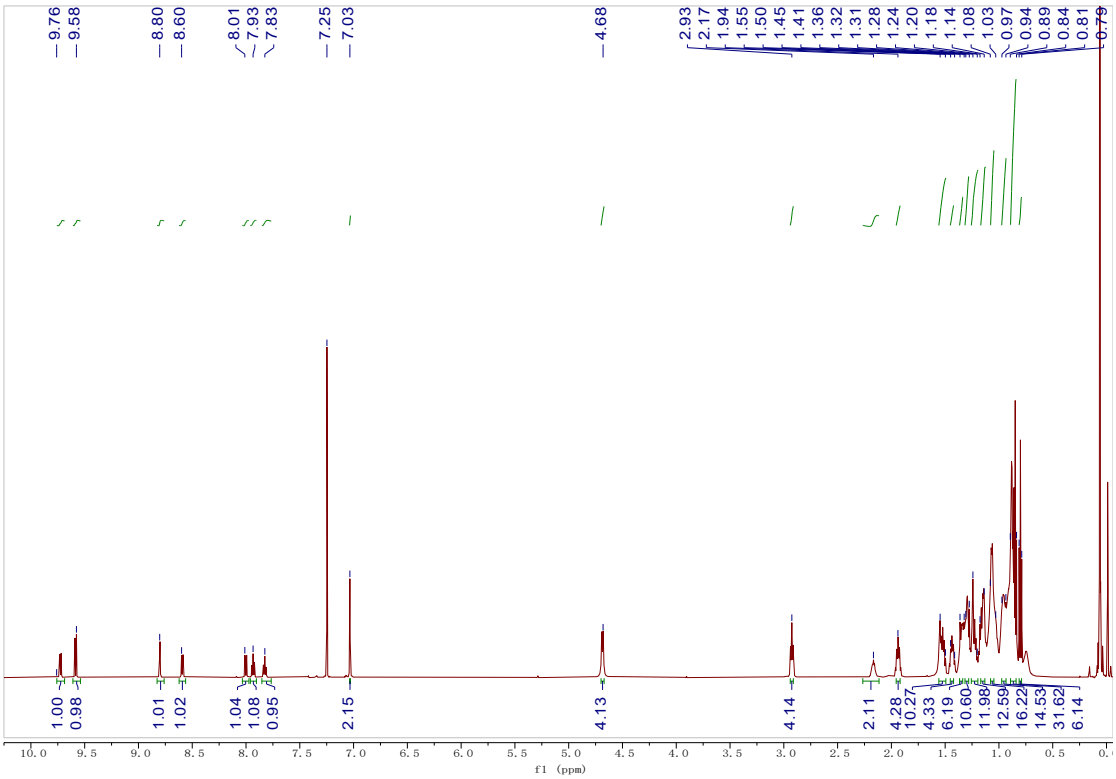

Figure S10. ^{1}H NMR spectra of Compound 3.

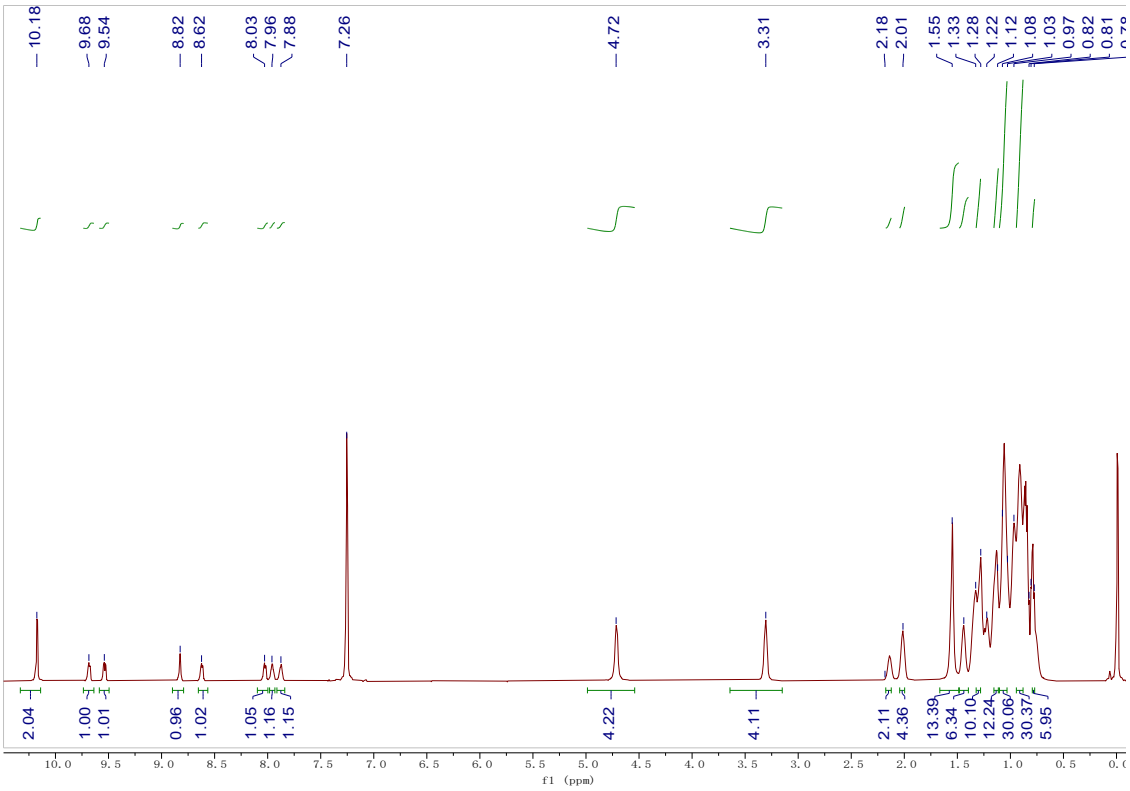

Figure S11. ^{1}H NMR spectra of Compound 4.

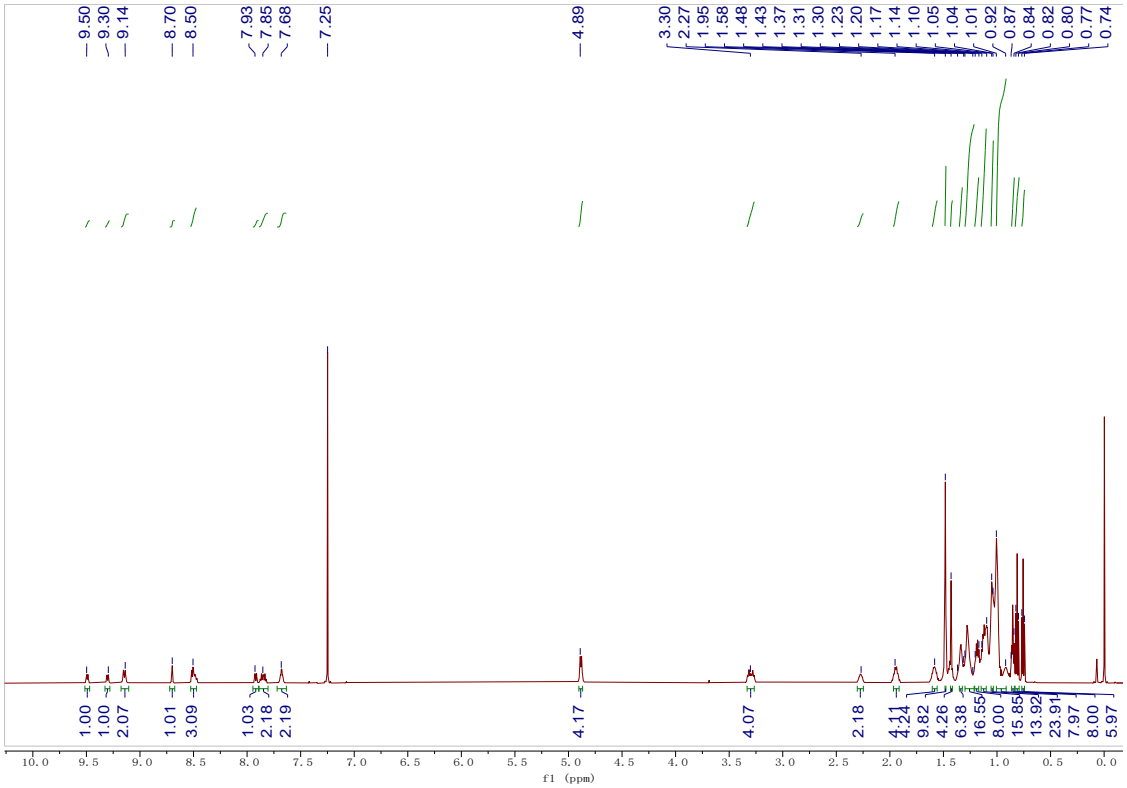

Figure S12. ^{1}H NMR spectra of PQx-F.

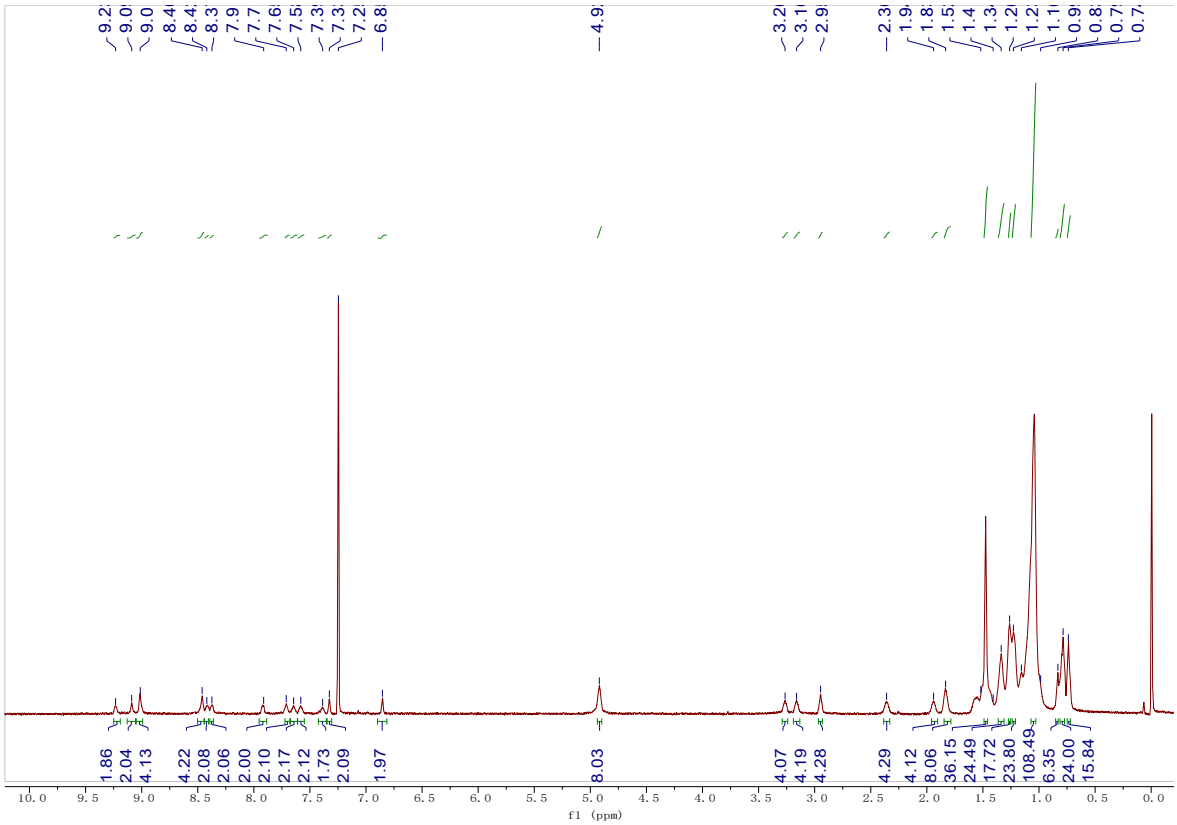

Figure S13. ^{1}H NMR spectra of *d*PQx-F.